STRUCTURAL BIOLOGY COMMUNICATIONS

ISSN 2053-230X

Crystal structure and kinetic analyses of a hexameric form of (*S*)-3-hydroxybutyryl-CoA dehydrogenase from *Clostridium acetobutylicum*

Mihoko Takenoya,[a] Seiichi Taguchi[b] and Shunsuke Yajima[a]*

[a]Department of Bioscience, Faculty of Life Sciences, Tokyo University of Agriculture, Setagaya-ku, Tokyo 156-8502, Japan, and [b]Department of Chemistry for Life Sciences and Agriculture, Faculty of Life Sciences, Tokyo University of Agriculture, 1-1-1 Sakuragaoka, Setagaya, Tokyo 156-8502, Japan. *Correspondence e-mail: yshun@nodai.ac.jp

Received 1 August 2018
Accepted 19 October 2018

Edited by I. Tanaka, Hokkaido University, Japan

Keywords: bio-based plastics; enzyme kinetics; fatty-acid metabolism; SDR superfamily; X-ray protein crystallography.

PDB references: (*S*)-3-hydroxybutyryl-CoA dehydrogenase from *C. acetobutylicum*, apo form, 6acq; NAD^+-bound form, 6aa8

Supporting information: this article has supporting information at journals.iucr.org/f

(*S*)-3-Hydroxybutyryl-CoA dehydrogenase (HBD) has been gaining increased attention recently as it is a key enzyme in the enantiomeric formation of (*S*)-3-hydroxybutyryl-CoA [(*S*)-3HB-CoA]. It converts acetoacetyl-CoA to (*S*)-3HB-CoA in the synthetic metabolic pathway. (*S*)-3HB-CoA is further modified to form (*S*)-3-hydroxybutyrate, which is a source of biodegradable polymers. During the course of a study to develop biodegradable polymers, attempts were made to determine the crystal structure of HBD from *Clostridium acetobutylicum* (CacHBD), and the crystal structures of both apo and NAD^+-bound forms of CacHBD were determined. The crystals belonged to different space groups: $P2_12_12_1$ and $P2_1$. However, both structures adopted a hexamer composed of three dimers in the asymmetric unit, and this oligomerization was additionally confirmed by gel-filtration column chromatography. Furthermore, to investigate the catalytic residues of CacHBD, the enzymatic activities of the wild type and of three single-amino-acid mutants were analyzed, in which the Ser, His and Asn residues that are conserved in the HBDs from *C. acetobutylicum*, *C. butyricum* and *Ralstonia eutropha*, as well as in the L-3-hydroxyacyl-CoA dehydrogenases from *Homo sapiens* and *Escherichia coli*, were substituted by alanines. The S117A and N188A mutants abolished the activity, while the H138A mutant showed a slightly lower K_m value and a significantly lower k_{cat} value than the wild type. Therefore, in combination with the crystal structures, it was shown that His138 is involved in catalysis and that Ser117 and Asn188 may be important for substrate recognition to place the keto group of the substrate in the correct position for reaction.

1. Introduction

Recently, emphasis on the use of environmentally friendly products has focused on the development of biodegradable polymers to replace nondegradable polymers that build up in soil and water. Biodegradable polymers have been synthesized in bacteria using metabolic pathway engineering (Hiraishi & Taguchi, 2009; Matsumoto & Taguchi, 2013). Such efforts will decrease the dependence on fossil fuel resources to produce plastics. Additionally, biodegradable polymers from sustainable materials such as corn, cane sugar, potato starch and tapioca starch can be made into polyesters and eventually recycled into soil (Shen *et al.*, 2010).

Several bio-based plastics have been produced utilizing renewable feedstocks. For example, homopolymers of lactate (LA) and 3-hydroxybutyrate (3HB) can be synthesized via a chemical/biological process and microbial fermentation, respectively. In the cases of the copolymers of LA and 3HB, the physical properties of the bioplastics can be varied by regulating the monomer composition and molecular weight in

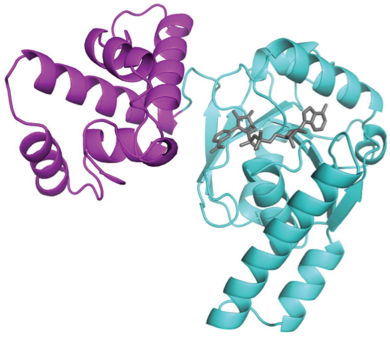

Table 1
Data-collection and refinement statistics.

Values in parentheses are for the outer shell.

	Apo	NAD^+ complex
Data collection		
Beamline	AR BL-NE3, PF	BL-17A, PF
Wavelength (Å)	1.000	0.980
Space group	$P2_12_12_1$	$P2_1$
Unit-cell parameters (Å, °)	a = 133.4, b = 134.5, c = 153.8	a = 77.4, b = 157.9, c = 81.8, α = 90.0, β = 100.9, γ = 90.0
Resolution range (Å)	50.0–2.50 (2.54–2.50)	50.0–2.10 (2.14–2.10)
Completeness (%)	100 (100)	98.6 (99.0)
$\langle I/\sigma(I)\rangle$	19.9 (1.9)	14.1 (2.0)
Multiplicity	6.7 (6.6)	2.2 (2.2)
R_{merge}† (%)	9.4 (68.5)	4.9 (31.6)
No. of unique reflections	95544	109647
Refinement		
Resolution range (Å)	47.9–2.50 (2.54–2.50)	48.46–2.10 (2.14–2.10)
No. of reflections	90674	104116
R/R_{free}‡ (%)	19.9/22.2	19.2/22.4
No. of atoms		
Protein	12912	12749
Solvent	79	404
Ligand (NAD^+)	—	88
R.m.s.d. from ideality		
Bond lengths (Å)	0.010	0.009
Bond angles (°)	1.326	1.308
Average B factor (Å^2)		
Protein	57.4	36.78
Solvent	40.4	31.7
Ligand (NAD^+)	—	49.4

† $R_{merge} = \sum_{hkl}\sum_i |I_i(hkl) - \langle I(hkl)\rangle| / \sum_{hkl}\sum_i I_i(hkl)$, where $I_i(hkl)$ is the ith measurement. ‡ A subset of the data (5%) was excluded from refinement and used to calculate R_{free}.

response to the desired applications (Taguchi *et al.*, 2008; Yamada *et al.*, 2010). For 3HB, which has enantiomeric isomers, only the *R*-form has been utilized. 3HB is synthesized *in vivo* starting from acetyl-CoA via two sequential enzymatic reactions. Two molecules of acetyl-CoA are first condensed to generate acetoacetyl-CoA by β-ketothiolase (PhaA). Acetoacetyl-CoA is then reduced to either (*R*)-3HB-CoA by an NADPH-dependent acetoacetyl-CoA reductase (PhaB) or to (*S*)-3HB-CoA by (*S*)-3-HB dehydrogenase (HBD). These compounds are stereoselectively converted to (*R*)-3HB and (*S*)-3HB, respectively, in living cells.

The development of an efficient monomer- and oligomer-production system in *Escherichia coli* using PhaB, which specifically synthesizes (*R*)-3HB-CoA, has been achieved (Oeding & Schlegel, 1973; Senior & Dawes, 1973; Kawaguchi & Doi, 1992; Matsumoto, Okei *et al.*, 2013). Furthermore, engineering of PhaB has successfully been achieved based on the tertiary structure of PhaB from *Ralstonia eutropha* (Matsumoto, Tanaka *et al.*, 2013). On the other hand, specific synthesis of (*S*)-3HB-CoA is not as commonly used as that of the CoA precursor of (*R*)-3HB, which is incorporated into the polymeric backbone (Boynton *et al.*, 1996; Lee *et al.*, 2008; Tseng *et al.*, 2009). Since (*S*)-3HB is useful as a building block for bioactive compounds such as antibiotics, the bioproduction of (*S*)-3HB has been extensively carried out in *E. coli* by the combination of HBD with a CoA-removing enzyme. In this context, we have focused on the HBD protein from *Clostridium acetobutylicum* (CacHBD) throughout our study of monomer production of (*S*)-3HB. In this paper, we report the crystal structures of apo CacHBD and the NAD^+-bound form of CacHBD, which exhibited a hexameric form that differs from those of the HBDs from *R. eutropha* and *C. butyricum*, the latter of which is highly homologous to CacHBD. A kinetic study also demonstrated the roles of catalytically important residues using single-amino-acid substituted mutants.

2. Materials and methods

2.1. Cloning, expression and purification of CacHBD

The gene encoding (*S*)-3-hydroxybutyryl-CoA dehydrogenase (EC 1.1.1.157) from *C. acetobutylicum* ATCC 824 (*Cachdb*; 843 bp) was amplified by polymerase chain reaction (PCR) using the synthesized *Cachbd* gene with codon optimization for *E. coli* as a template. The PCR product was cloned into pET-28b(+) (Novagen) with an N-terminal 6×His tag using NdeI and XhoI restriction enzymes. Consequently, the extra sequence MGSSHHHHHHSSGLVPRGSH was added to the N-terminus of the recombinant enzyme. This expression plasmid was transformed into the Rosetta 2(DE3) *E. coli* strain. To prepare the single amino-acid mutants (S117A, H138A and N188A), the pET28b-*Cachbd* plasmid was used as a template. The following primers were used to introduce point mutations into pET-28b-*Cachbd* by PCR: 5′-ACCGCGTCTCTGTCTATCACC-3′ and 5′-AGAGACGCG GTGTTAGACGC-3′ were used for S117A, 5′-TATGGCGTT CTTCAACCCGGCGCCG-3′ and 5′-AGAACGCCATACCG ATAACTTTGTC-3′ were used for H138A and 5′-TTGCG CGTATCCTGATCCCGATGATC-3′ and 5′-ATACGCGCA ACAACGAAACCCGGCG-3′ were used for N188A. Each mutation that was introduced was confirmed by sequencing.

E. coli cells harboring the expression plasmid were cultured in Luria–Bertani (LB) broth medium containing 25 µg ml^{-1} kanamycin and 34 µg ml^{-1} chloramphenicol at 20°C. After 8 h of culture, 250 µ*M* (final concentration) isopropyl β-D-1-thiogalactopyranoside (IPTG) was added for induction of the target protein. The culture was then continued for 16 h and the cells were harvested by centrifugation at 4648*g* for 15 min at 4°C.

The cells were resuspended in buffer consisting of 20 m*M* Tris–HCl pH 7.5, 20 m*M* imidazole, 200 m*M* NaCl and were homogenized by ultrasonication. The supernatant that was separated by centrifugation at 69 673*g* for 40 min was purified using an Ni cOmplete column (Roche) and an anion-exchange Mono Q column (GE Healthcare Bio). The purified CacHBD was then concentrated to 30 mg ml^{-1} by ultrafiltration with Amicon Ultra (Millipore).

2.2. Crystallization

Crystallization was performed using the hanging-drop vapor-diffusion method at 20°C for both apo and NAD^+-bound CacHBD. In the case of NAD^+-bound CacHBD, a final concentration of 5 m*M* NAD^+ was added to 30 mg ml^{-1} protein solution. The protein solution and reservoir solution

were mixed in a 1:1 ratio. After optimization of the reservoir condition, NAD^+-bound crystals grew to dimensions of 0.4 × 0.1 × 0.1 mm using a reservoir solution consisting of 17.5% PEG 3350, 200 m*M* sodium thiocyanate. Apo crystals grew to dimensions of 0.4 × 0.2 × 0.2 mm using a reservoir solution consisting of 1.25% PEG 400, 2.2 *M* ammonium sulfate, 0.1 *M* HEPES–NaOH pH 7.5.

2.3. Data collection and structure determination

Crystals were flash-cooled in liquid nitrogen using nylon loops without a cryoprotectant solution. Diffraction data were collected on beamlines BL-17A and AR BL-NE3 at the Photon Factory (PF), Tsukuba, Japan. Indexing, integration, scaling and merging were carried out using *HKL*-2000 (Otwinowski & Minor, 1997).

The initial structure of NAD^+-bound CacHBD was determined by the molecular-replacement method using *MOLREP* (Vagin & Teplyakov, 2010). The structure of HBD from *C. butyricum* (CbuHBD; PDB entry 4r1n; Kim, Kim *et al.*, 2014) served as a search model since the sequence identity of HBD between *C. acetobutylicum* and *C. butyricum* is 81.2%. The model was then constructed using *ARP*/*wARP* (Langer *et al.*, 2008). Further iterative refinement and model building were conducted with *REFMAC*5 (Murshudov *et al.*, 2011) and *Coot* (Emsley *et al.*, 2010), respectively. All programs apart from *HKL*-2000 and *Coot* were used within the *CCP*4 suite (Winn *et al.*, 2011). The structure of apo CacHBD was determined by molecular replacement using the NAD^+-bound structure as a search model. Data-collection and refinement statistics are summarized in Table 1.

2.4. Gel-filtration chromatography

A Superdex 200 Increase 10/300 GL column (GE Healthcare Bio) was used to calculate the molecular weight of CacHBD in solution. The column was equilibrated with buffer consisting of 50 m*M* HEPES–NaOH pH 7.5, 150 m*M* NaCl. Ferritin (440 kDa), aldolase (158 kDa), conalbumin (75 kDa) and ovalbumin (43 kDa) from Gel Filtration Calibration Kit HMW (GE Healthcare Bio) were used as molecular markers.

2.5. Enzyme assay

The enzymatic activity of CacHBD was measured by the oxidation of NADH to NAD^+ and was monitored by spectroscopy at 340 nm using a V-750ST spectrophotometer (Jasco) equipped with a CTU-100 circulating thermostat unit (Jasco). The total volume of the reaction mixture was 1 ml; it contained 0.1 *M* HEPES–NaOH pH 7.5 and 200 µ*M* NADH to determine the kinetic parameters of acetoacetyl-CoA or 50 µ*M* acetoacetyl-CoA instead of NADH to determine the kinetic parameters of NADH. The reaction buffer was pre-incubated for 2 min at 37°C, followed by serial additions of NADH, 10 n*M* (wild type) or 1 µ*M* (mutants) CacHBD and acetoacetyl-CoA to initiate the reaction. Acetoacetyl-CoA at 10, 20, 30, 40, 50 and 100 µ*M*, and NADH at 10, 20, 50, 100, 150 and 200 µ*M* were used to determine the kinetic parameters. Each reaction was performed in triplicate. The data were confirmed to fit to the Michaelis–Menten equation and the parameters were calculated using a Lineweaver–Burk plot.

3. Results and discussion

3.1. Overall structure

The crystal structures of the apo and NAD^+-bound forms of CacHBD were determined at 2.5 and 2.1 Å resolution, respectively. As expected, the overall structures of CacHBD and CbuHBD were essentially identical. When the monomer subunits of apo CacHBD and apo CbuHBD were superposed, the r.m.s.d. value (calculated for C^α atoms) was 0.73 Å, as calculated by *Chimera* (Pettersen *et al.*, 2004). The monomer structure consisted of two domains. The N-terminal domain consisted of a Rossmann fold, which binds to NAD^+ (Fig. 1*a*), and the C-terminal domain formed a dimer interface in the crystal structure (Fig. 1*b*). The apo and NAD^+-bound CacHBD crystals belonged to space groups $P2_12_12_1$ and $P2_1$, respectively. In the asymmetric unit, both crystals contained three dimers of CacHBD forming a hexamer, which belonged to point-group symmetry *D*3 with a pseudo-threefold axis and three twofold axes (Fig. 1*c*). On the other hand, the CbuHBD crystal belonged to space group *H*3, and two and four dimers were present in the asymmetric unit for the apo (PDB entry 4r1n) and substrate-bound forms (PDB entry 4kuh), respectively. Space group *H*3 also has threefold symmetry, and we confirmed that the CbuHBD structures are also able to form the same hexamer as in CacHBD in the unit cell. However, CbuHBD was reported to form a dimer in a gel-filtration experiment (Kim, Kim *et al.*, 2014). Therefore, we analyzed the oligomerization state of CacHBD in solution using gel-filtration column chromatography, which revealed that the calculated state was a 7.3-mer (Supplementary Fig. S1). It is therefore highly possible that CacHBD forms a hexamer in solution. The differences in buffer conditions between the experiments could have affected the oligomerization state; however, the cause of the difference in the oligomerization states could not be confirmed as the buffer conditions were not mentioned by Kim, Kim *et al.* (2014).

3.2. Comparison of monomer subunits of hexameric CacHBD

The crystal structures obtained in this study were composed of two types of dimers: a homodimer of two apo subunits and a heterodimer of NAD^+-bound and apo subunits. No homodimers of NAD^+-bound subunits were obtained. Therefore, three types of subunits existed: an apo subunit (type A) from a homodimer and an NAD^+-bound subunit (type B) and an apo subunit (type C) from a heterodimer. When the C-terminal domains of the 12 monomers of apo and NAD^+-bound CacHBD in the asymmetric units were superposed, they were essentially identical (Fig. 2*a*, middle). However, one difference was observed for Glu90 in loop 1 containing Ala87–Arg91, as shown in Fig. 2(*a*). The side chains of Glu90 were flipped in two of the 12 monomers. These two subunits were type C. Among the 12 subunits in a hexamer, only two subunits bound to NAD^+, and their counterpart subunits in the dimers did not

bind to NAD^+. The difference was caused by the mode of interaction of Glu90. In type A, Glu90 interacted with Thr116 and Ser118, forming hydrogen bonds with distances of 2.6 and 2.7 Å, respectively (Fig. 2*b*, left). Glu90 in type B also formed hydrogen bonds to Thr116, Ser117, Ser118 and NAD^+ at distances of 2.5, 3.0, 2.9 and 2.7 Å, respectively (Fig. 2*b*, middle). On the other hand, type C subunits made no apparent interactions with other residues (Fig. 2*b*, right).

Furthermore, we examined the temperature factors of loop 1 (consisting of Ala87–Arg91) and loop 2 (consisting of Asn115–Ser120). When loop 1 interacted with loop 2 in type A subunits, the temperature factors of loops 1 and 2 had high and low values, respectively (Fig. 2*c*, left). In type B subunits, the temperature factors of both loops were lower (Fig. 2*c*, middle). In type C subunits, which exhibited no interactions between loop 1 and loop 2, the temperature factors of both loops were higher (Fig. 2*c*, right). Although the corresponding Glu residues are located at the nonflipped position in the case of the crystal structures of CbuHBD, the results suggest that loop 1 retains the flexibility to accept NAD^+. Upon the binding of NAD^+, loop 1 becomes more stable than that in apo CacHBD.

3.3. Comparison of monomer subunits between CacHBD and L-3-hydroxyacyl-CoA dehydrogenase from *Homo sapiens*

L-3-Hydroxyacyl-CoA dehydrogenase from *H. sapiens* (HuHAD) has acetoacetyl-CoA reductase activity (Barycki *et al.*, 1999), and the crystal structure was determined as a

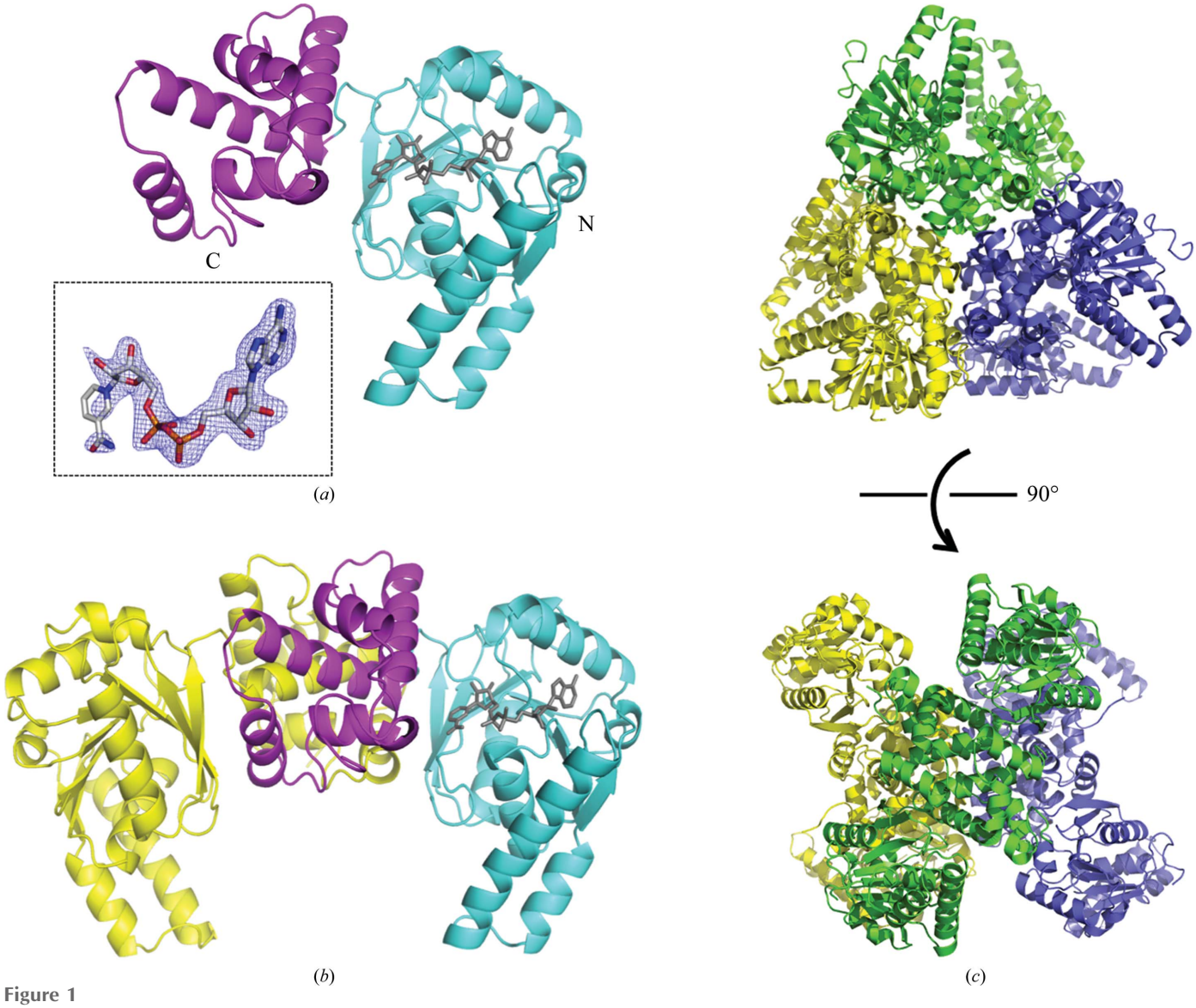

Figure 1
Overall structure of HBD from *C. acetobutylicum* (CacHBD). The structures are shown as (*a*) a monomer, (*b*) a dimer and (*c*) a hexamer containing three dimers in the asymmetric unit. (*a*) In the monomeric form the N- and C-terminal domains are colored cyan and magenta, respectively. NAD^+ is shown as a gray stick model. In the inset, the $F_o - F_c$ OMIT map contoured at 3σ for NAD^+ is represented as a blue mesh; it was calculated by excluding the NAD^+ molecule. (*b*) In the dimeric form one monomer is shown in the same colors as in (*a*) and the other is shown in yellow. (*c*) In the hexameric form in the asymmetric unit, the dimers are shown in yellow, green and purple. The top and bottom views are shown from the pseudo-threefold and twofold axis directions, respectively.

ternary complex with NAD^+ and acetoacetyl-CoA (PDB entry 1f0y; Barycki *et al.*, 2000). Furthermore, crystal structures of HuHAD in the apo form (PDB entry 1f14) and in a binary form with NADH (PDB entry 1f17) have been determined (Barycki *et al.*, 2000). These three crystal structures of HuHAD and the apo and NAD^+-bound CacHBD structures were superposed. A significant difference was observed between apo CacHBD and the ternary complex of HuHAD. The other structures were similar to that of apo CacHBD. In this study, the N-terminal domains of the ternary complex of HuHAD and apo CacHBD were superposed using *Chimera* (Fig. 3). The r.m.s.d. value (calculated for C^α atoms) of the N-terminal domain was 0.77 Å (residues 1–188 in the N-terminus of CacHBD and residues 15–208 in the N-terminus of HuHAD). In this case, the r.m.s.d. value of the C-terminal domains was 7.50 Å over 93 residues (residues 189–281 in the C-terminus of CacHBD and residues 209–301 in the C-terminus of HuHAD). Since the N- and C-terminal domains of the ternary complex of HuHAD adopted a closed conformation compared with those of apo CacHBD, the distances between the N-terminal and C-terminal domains were measured using the amino acids located at the corresponding positions in the crystal structures. The distance between Thr11 in the N-terminal domain and Lys272 in the C-terminal domain of apo CacHBD was 14.2 Å. Meanwhile, in the ternary complex of HuHAD the distance between Leu25 in the N-terminal domain and Lys293 in the C-terminal domain was 8.0 Å (Fig. 3). A large domain movement therefore seemed to be induced upon the binding of acetoacetyl-CoA rather than upon that of NAD^+.

3.4. The NAD^+-binding site of CacHBD

In the CacHBD structure from the $P2_1$ crystal, only two subunits in the hexamer were observed to bind to NAD^+. In the binding mode for NAD^+, Thr11, Met12, Arg30, Asp31, Arg39, Glu90, Lys95, Asn115 and Ser117 formed hydrogen bonds to NAD^+ in both or either of the subunits. On the other hand, the same residues as in CacHBD, except for Arg39, are involved in hydrogen bonds in CbuHBD (PDB entry 4kug;

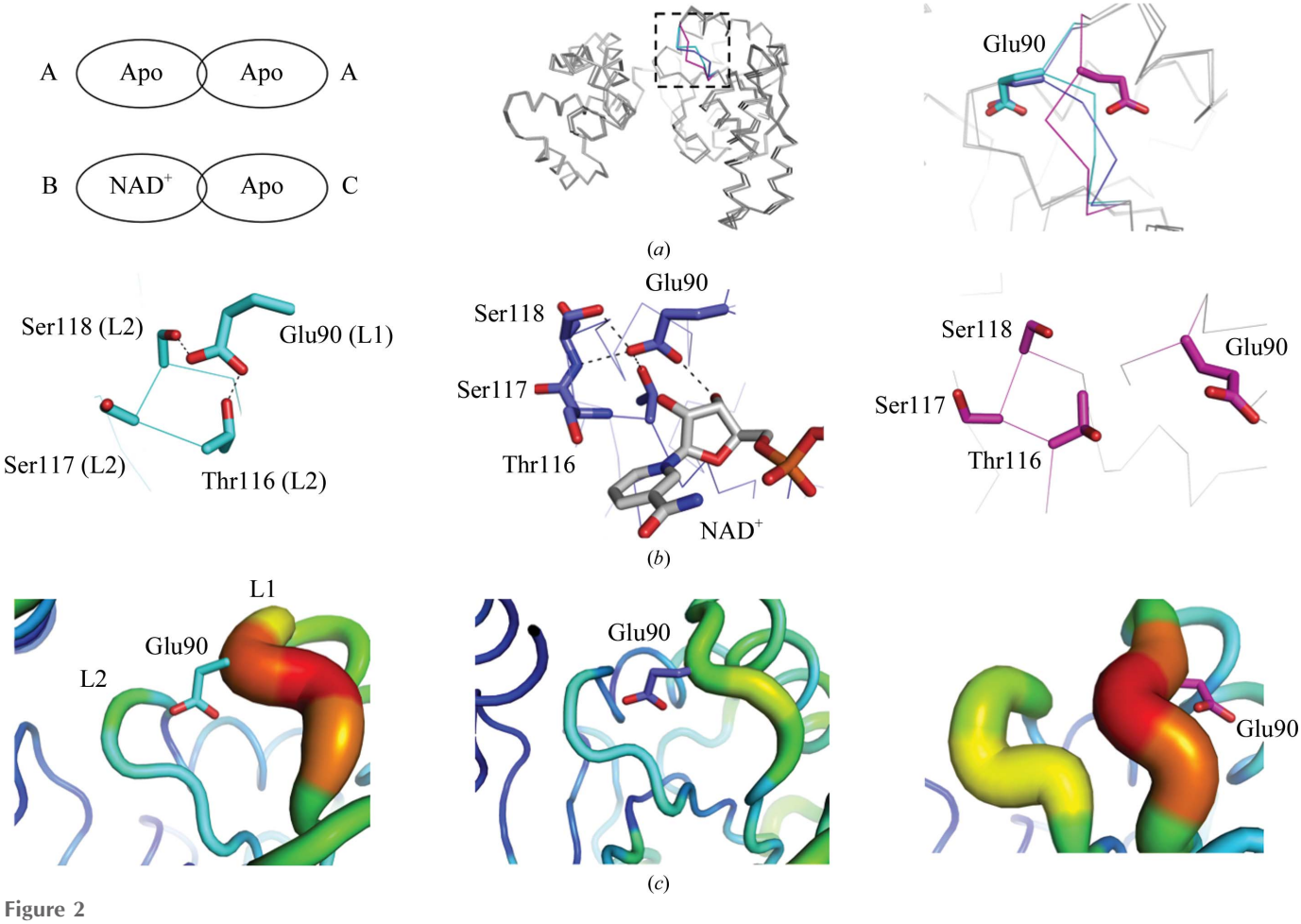

Figure 2
Comparison of the monomer subunits in CacHBD. (*a*) Two types of dimers were found in the CacHBD crystal structures. They are schematically represented and the subunits are denoted as types A, B and C (left). 12 monomers in the asymmetric units of apo CacHBD and NAD^+-bound CacHBD are superposed on the C-terminal domains. In the loop 1 region consisting of Ala87–Arg91, types A, B and C are partly colored cyan, blue and magenta, respectively (middle). Part of the dotted square in the middle panel is enlarged in the right panel. (*b*) Residues interacting with Glu90 are represented as stick models. The left, middle and right panels correspond to subunit types A, B and C, respectively. Dotted lines in the left and middle panels represent hydrogen bonds. (*c*) The *B* factor is shown in color, as prepared by *PyMOL* (Schrödinger). The highest and lowest values are shown in red and blue, respectively, with a gradient of colors in between. Each panel is viewed from the same direction as that in (*b*).

Table 2
Kinetic parameters for HBD from *C. acetobutylicum*.

ND; not detectable for calculations.

	NADH			Acetoacetyl-CoA		
CacHBD	K_m (μ*M*)	k_{cat} (s^{-1})	k_{cat}/K_m (μ*M* s^{-1})	K_m (μ*M*)	k_{cat} (s^{-1})	k_{cat}/K_m (μ*M* s^{-1})
Wild type	31.4 ± 4.9	$8.5 \times 10^3 \pm 9.3 \times 10^2$	$2.7 \times 10^2 \pm 1.2 \times 10$	22.7 ± 4.6	$1.3 \times 10^4 \pm 1.1 \times 10^3$	$6.3 \times 10^2 \pm 8.0 \times 10$
S117A	ND	ND	ND	ND	ND	ND
H138A	16.8 ± 1.2	93.8 ± 1.9	5.6 ± 0.3	9.6 ± 0.9	104.3 ± 2.2	11.0 ± 0.7
N188A	ND	ND	ND	ND	ND	ND

Kim, Kim *et al.*, 2014). When the crystal structures were superposed using *Chimera*, they fitted well with an r.m.s.d. value of 0.88 Å (calculated on C^{α} atoms), and the binding modes for NAD^+ in both proteins were almost identical, with a slight difference in the directions of the side chains of the amino-acid residues (Fig. 4). These differences may reflect the flexibility of the side chains of the residues and/or the differences in the resolutions of the crystal structures: 2.3 and 2.1 Å for CbuHBD and CacHBD, respectively. In addition to the hydrogen bonds formed, the adenine moiety of NAD^+ was positioned in a hydrophobic pocket formed by Leu7, Ile32, Ala88, Val89, Ile94 and Ile98 in CacHBD. This pocket was also observed in CbuHBD (Kim, Kim *et al.*, 2014), with a single difference of Val89 in CacHBD compared with Ile89 in CbuHBD.

3.5. Enzymatic activity

To characterize the properties of CacHBD, a kinetic analysis was performed with acetoacetyl-CoA as a substrate. The resulting K_m values for acetoacetyl-CoA and NADH were 22.7 and 31.4 μ*M*, respectively. The k_{cat} values for acetoacetyl-CoA and NADH were 1.3×10^4 and 8.5×10^3 s^{-1}, respectively (Table 2). These values were most comparable to those of HBD from *R. eutropha* (PaaH), with a K_m of 18.5 μ*M* and a k_{cat} of 4.55×10^5 s^{-1} for acetoacetyl-CoA. The values for CbuHBD are a K_m of 28 μ*M* and a k_{cat} of 3.4×10^3 min^{-1} for the substrate. The difference in the k_{cat} values between CbuHBD and CacHBD may have resulted from the varying temperatures of the reactions (37 and 30°C for CacHBD and CbuHBD, respectively).

The residues involved in the catalytic activities were investigated. With regard to L-3-hydroxyacyl-CoA dehydrogenase from *E. coli* (EcHAD), based on the sequence alignment, a single-amino-acid mutation of His450 corresponding to His138 in CacHBD (Fig. 5*a*), which was substituted by alanine, dramatically decreased the k_{cat} value with acetoacetyl-CoA as a substrate without changing the K_m value (He & Yang, 1996). Barycki and coworkers reported the ternary-complex structure of human L-3-hydroxyacyl-CoA dehydrogenase with acetoacetyl-CoA and NAD^+ and proposed that Ser149 (corresponding to Ser117 in CacHBD), His170 (His138) and Asn220 (Asn188) may be important for catalytic activity (Barycki *et al.*, 2000). Kim, Chang *et al.* (2014)

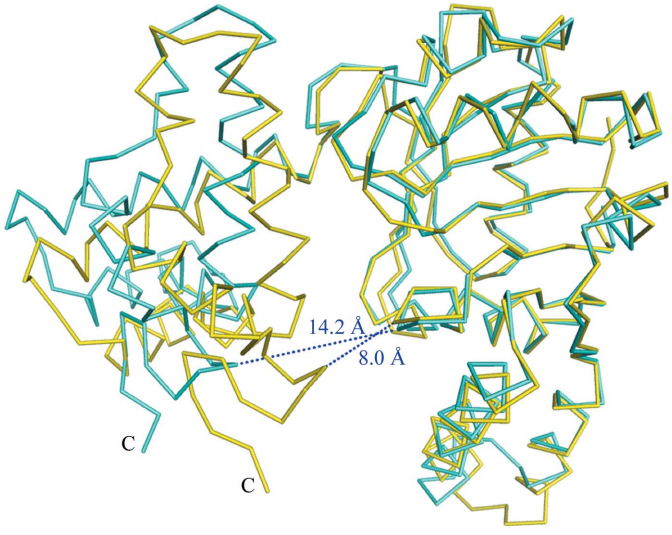

Figure 3
Comparison of monomer subunit structures between the NAD^+-bound form of CacHBD (this study) and the ternary complex of HuHAD with NAD^+ and acetoacetyl-CoA (PDB entry 1f0y). The NAD^+-bound form of CacHBD and the ternary complex of HuHAD are superposed on the N-terminal domains and are colored cyan and yellow, respectively. Blue dotted lines indicate the distances (labeled) between the N-terminal and C-terminal domains in each structure.

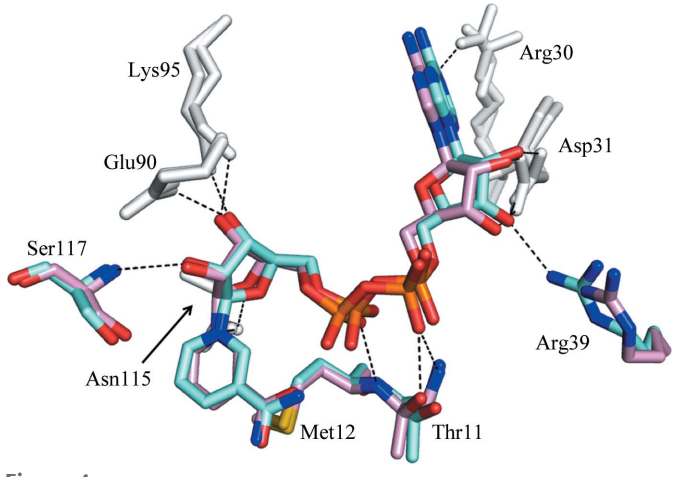

Figure 4
Superposition of the NAD^+-binding sites of CacHBD and CbuHBD. One of the two subunits of the NAD^+-bound form of CacHBD (this study) and one of the four subunits of CbuHBD (PDB entry 4kug; Kim, Kim *et al.*, 2014) are superposed and are colored cyan and pink, respectively, using *Chimera*. Residues colored gray represent the positions where hydrogen bonds are formed to NAD^+ in all six subunits (two from CacHBD and four from CbuHBD). Residues colored cyan or pink indicate that the formation of hydrogen bonds depends on the subunits of both HBDs, with the exception that Arg39 formed a hydrogen bond to NAD^+ only in CacHBD. Hydrogen bonds are represented by black dotted lines.

```
CacHBD  110 TILASNTSSLSITEVASATKRPDKVIGMHFFNPAP 144   180 AEAPGFVVNRILIP  193
CbuHBD  110 TILASNTSSLSITEVASATKRADKVIGMHFFNPAP 144   180 AEAPGFVVNRILIP  193
PaaH    112 VIIASNTSSISITKLAAVTSRADRFIGMHFFNPVP 146   182 KNSPGFVVNRILCP  195
HuHAD   142 TIFASNTSSLQITSIANATTRQDRFAGLHFFNPVP 176   212 KDTPGFIVNRLLVP  225
EcHAD   422 TVLASNTSTIPISELANALERPENFCGMHFFNPVH 456   492 NDCPGFFVNRVLFP  505
                *****   *   *    *     * *****           *** *** * *
```

(*a*)

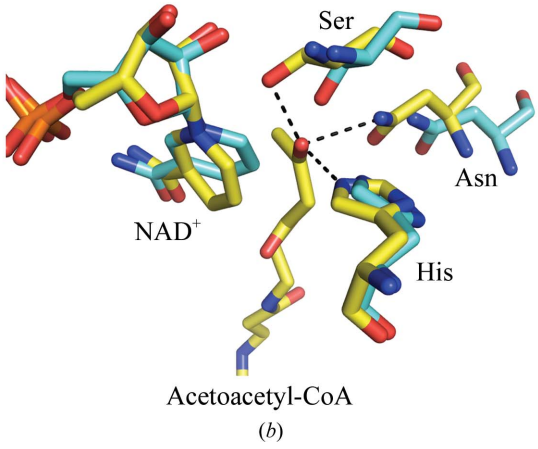

(*b*)

Figure 5
Putative catalytic residues of CacHBD, CbuHBD, PaaH, HuHAD and EcHAD. (*a*) Amino-acid sequence alignment of (*S*)-3-hydroxybutyryl-CoA dehydrogenase (HBD) from *C. acetobutylicum* (CacHBD), HBD from *C. butyricum* (CbuHBD), HBD from *R. eutropha* (PaaH), L-3-hydroxyacyl-CoA dehydrogenase from *H. sapiens* (HuHAD) and HAD from *E. coli* (EcHAD). Asterisks represent residues that are conserved among sequences. The mutated Ser, His and Asn residues are shown in red. (*b*) The crystal structure of NAD^+-bound CacHBD is superposed on that of the ternary HuHAD complex. CacHBD and HuHAD are shown in cyan and yellow, respectively. Ser, His and Asn, shown as stick models, correspond to the residues colored red in (*a*). Black dotted lines show the distances between the keto oxygen and Ser (2.5 Å), Asn (2.9 Å) and His (2.6 Å) in HuHAD.

followed up these facts by introducing single-amino-acid substitutions of Ser119 (corresponding to Ser117 in CacHBD) and Asn190 (Asn188) by alanines in HBD from *R. eutropha*. The activities relative to the wild type were measured and exhibited a significant decrease (Kim, Chang *et al.*, 2014). Therefore, in order to compare the activities and confirm the roles of these residues in CacHBD, we introduced single-amino-acid substitutions of Ser117, His138 and Asn188 by alanines. The H138A mutant showed a marked decrease in the k_{cat} value but not the K_m value, indicating a role in catalysis. Meanwhile, the k_{cat} and K_m values could not be calculated for the S117A and N188A mutants owing to very low activities. These two residues may therefore be important for substrate binding, especially in placing the keto group in the correct position for reaction (Fig. 5*b*). In turn, this might reflect the fact that kinetic values for NADH were also not obtained.

Acknowledgements

We thank Dr Ken'ichiro Matsumoto for providing us with a synthetic gene for CacHBD and for critical reading of the manuscript. We also thank the staff of the Photon Factory for assistance during data collection.

References

Barycki, J. J., O'Brien, L. K., Bratt, J. M., Zhang, R., Sanishvili, R., Strauss, A. W. & Banaszak, L. J. (1999). *Biochemistry*, **38**, 5786–5798.
Barycki, J. J., O'Brien, L. K., Strauss, A. W. & Banaszak, L. J. (2000). *J. Biol. Chem.* **35**, 27186–27196.
Boynton, Z. L., Bennet, G. N. & Rudolph, F. B. (1996). *J. Bacteriol.* **178**, 3015–3024.
Emsley, P., Lohkamp, B., Scott, W. G. & Cowtan, K. (2010). *Acta Cryst.* D**66**, 486–501.
He, X.-Y. & Yang, S.-Y. (1996). *Biochemistry*, **35**, 9625–9630.
Hiraishi, T. & Taguchi, S. (2009). *Mini-Rev. Org. Chem.* **6**, 44–54.
Kawaguchi, U. & Doi, Y. (1992). *Macromolecules*, **25**, 2324–2329.
Kim, E.-J., Kim, J., Ahn, J.-W., Kim, Y.-J., Chang, J. H. & Kim, K.-J. (2014). *J. Microbiol. Biotechnol.* **24**, 1636–1643.
Kim, J., Chang, J. H. & Kim, K.-J. (2014). *Biochem. Biophys. Res. Commun.* **448**, 163–168.
Langer, G., Cohen, S. X., Lamzin, V. S. & Perrakis, A. (2008). *Nature Protoc.* **3**, 1171–1179.
Lee, S.-H., Park, S. J., Lee, S. Y. & Hong, S. H. (2008). *Appl. Microbiol. Biotechnol.* **79**, 633–641.
Matsumoto, K., Okei, T., Honma, I., Ooi, T., Aoki, H. & Taguchi, S. (2013). *Appl. Microbiol. Biotechnol.* **97**, 205–210.
Matsumoto, K. & Taguchi, S. (2013). *Curr. Opin. Biotechnol.* **24**, 1054–1060.
Matsumoto, K., Tanaka, Y., Watanabe, T., Motohashi, R., Ikeda, K., Tobitani, K., Yao, M., Tanaka, I. & Taguchi, S. (2013). *Appl. Environ. Microbiol.* **79**, 6134–6139.
Murshudov, G. N., Skubák, P., Lebedev, A. A., Pannu, N. S., Steiner, R. A., Nicholls, R. A., Winn, M. D., Long, F. & Vagin, A. A. (2011). *Acta Cryst.* D**67**, 355–367.
Oeding, V. & Schlegel, H. G. (1973). *Biochem. J.* **134**, 239–248.
Otwinowski, Z. & Minor, W. (1997). *Methods Enzymol.* **276**, 307–326.
Pettersen, E. F., Goddard, T. D., Huang, C. C., Couch, G. S., Greenblatt, D. M., Meng, E. C. & Ferrin, T. E. (2004). *J. Comput. Chem.* **25**, 1605–1612.
Senior, P. J. & Dawes, E. A. (1973). *Biochem. J.* **134**, 225–238.
Shen, L., Worrell, E. & Patel, M. (2010). *Biofuel. Bioprod. Bioref.* **4**, 25–40.
Taguchi, S., Yamada, M., Matsumoto, K., Tajima, K., Satoh, Y., Munekata, M., Ohno, K., Kohda, K., Shimamura, T., Kambe, H. & Obata, S. (2008). *Proc. Natl Acad. Sci. USA*, **105**, 17323–17327.

Tseng, H.-C., Martin, C. H., Nielsen, D. R. & Prather, K. L. J. (2009). *Appl. Environ. Microbiol.* **75**, 3137–3145.
Vagin, A. & Teplyakov, A. (2010). *Acta Cryst.* D**66**, 22–25.
Winn, M. D., Ballard, C. C., Cowtan, K. D., Dodson, E. J., Emsley, P., Evans, P. R., Keegan, R. M., Krissinel, E. B., Leslie, A. G. W., McCoy, A., McNicholas, S. J., Murshudov, G. N., Pannu, N. S., Potterton, E. A., Powell, H. R., Read, R. J., Vagin, A. & Wilson, K. S. (2011). *Acta Cryst.* D**67**, 235–242.
Yamada, M., Matsumoto, L., Shimizu, K., Uramoto, S., Nakai, T., Shozui, F. & Taguchi, S. (2010). *Biomacromolecules*, **11**, 815–819.